

## RESEARCH ARTICLE

10.1029/2019JE005951

## Key Points:

- The Portales Valley H6 chondrite experienced a magnetic field with properties consistent with dynamo fields at 100 Myr after CAI formation
- This observation indicates that the H chondrite parent body contained an advecting metallic core, so was partially differentiated
- We model the thermal evolution of such bodies, finding that they can reproduce the measured ages and cooling rates of multiple H chondrites

## Supporting Information:

- Supporting Information S1

## Correspondence to:

J. F. J. Bryson,  
jfb2@cam.ac.uk

## Citation:

Bryson, J. F. J., Weiss, B. P., Getzin, B., Abrahams, J. N. H., Nimmo, F., & Scholl, A. (2019). Paleomagnetic evidence for a partially differentiated ordinary chondrite parent asteroid. *Journal Geophysical Research: Planets*, 124, 1880–1898. <https://doi.org/10.1029/2019JE005951>

Received 21 FEB 2019

Accepted 12 APR 2019

Accepted article online 19 JUN 2019

Published online 18 JUL 2019

## Author Contributions

**Conceptualization:** J. F. J. Bryson, B. P. Weiss

**Data curation:** J. F. J. Bryson

**Funding Acquisition:** B. P. Weiss

**Methodology:** J. F. J. Bryson

**Writing - Original Draft:** J. F. J. Bryson, B. P. Weiss, F. Nimmo

**Formal Analysis:** J. F. J. Bryson, B. Getzin, J. N. H. Abrahams, F. Nimmo

**Investigation:** J. F. J. Bryson, B. Getzin, J. N. H. Abrahams, F. Nimmo

**Project Administration:** B. P. Weiss

# Paleomagnetic Evidence for a Partially Differentiated Ordinary Chondrite Parent Asteroid

J. F. J. Bryson<sup>1,2</sup>, B. P. Weiss<sup>1</sup>, B. Getzin<sup>3</sup>, J. N. H. Abrahams<sup>4,5</sup>, F. Nimmo<sup>5</sup>, and A. Scholl<sup>6</sup>

<sup>1</sup>Department of Earth, Atmospheric and Planetary Sciences, Massachusetts Institute of Technology, Cambridge, MA, USA, <sup>2</sup>Department of Earth Sciences, University of Cambridge, Cambridge, UK, <sup>3</sup>Smith College, Northampton, MA, USA, <sup>4</sup>Division of Geological and Planetary Sciences, California Institute of Technology, Pasadena, CA, USA, <sup>5</sup>Department of Earth and Planetary Sciences, University of California, Santa Cruz, Santa Cruz, CA, USA, <sup>6</sup>Advanced Light Source, Lawrence Berkeley National Laboratory, Berkeley, CA, USA

**Abstract** The textures and accretion ages of chondrites have been used to argue that their parent asteroids never differentiated. Without a core, undifferentiated planetesimals could not have generated magnetic fields through dynamo activity, so chondrites are not expected to have experienced such fields. However, the magnetic remanence carried by the CV chondrites is consistent with dynamo-generated fields, hinting that partially differentiated asteroids consisting of an unmelted crust atop a differentiated interior may exist. Here, we test this hypothesis by applying synchrotron X-ray microscopy to metallic veins in the slowly cooled H6 chondrite Portales Valley. The magnetic remanence carried by nanostructures in these veins indicates that this meteorite recorded a magnetic field over a period of tens to hundreds of years at ~100 Myr after solar system formation. These properties are inconsistent with external field sources such as the nebula, solar wind, or impacts, but are consistent with dynamo-generated fields, indicating that the H chondrite parent body contained an advecting metallic core and was therefore partially differentiated. We calculate the thermal evolution of the chondritic portions of partially differentiated asteroids that form through incremental accretion across  $10^5$  to  $10^6$  years, finding this can agree with the measured ages and cooling rates of multiple H chondrites. We also predict that the cores of these bodies could have been partially liquid and feasibly generating a dynamo at 100 Myr after solar system formation. These observations contribute to a growing body of evidence supporting a spectrum of internal differentiation within some asteroids with primitive surfaces.

**Plain Language Summary** Asteroids formed during the first few million years of the solar system through the accretion of billions of millimeter-sized solids. If this process occurred within the first ~2 Myr of the solar system, the asteroid is thought to have partially melted, while if it occurred after this time, the asteroid is thought to have remained completely unmelted. Partial melting is an easy mechanism allowing an asteroid to differentiate into a rocky mantle and metallic core. Recently, this discrete nature of asteroid melting has been challenged by magnetic measurements of a group of unmelted meteorites that suggest they experienced magnetic fields generated in an asteroid core, hinting that their parent asteroid contained both melted and unmelted material and was therefore partially differentiated. Here, we show that a previously unmeasured type of unmelted meteorite recorded a magnetic field over a period of tens to hundreds of years at ~100 million years after solar system formation. These timings make this a particularly robust observation that some unmelted meteorites experienced dynamo fields and originate from partially differentiated asteroids. This observation favors the episodic formation of some asteroids, potentially impacting our understanding of the thermal and structural history of the first planetary bodies in our solar system.

## 1. Introduction

Meteorites are classified into two primary petrographic types: chondrites, which are aggregates of nebular materials that remained unmelted on their parent planetesimals, and achondrites, which are the products of planetesimal melting processes (Weiss & Elkins-Tanton, 2013). A planetesimal's thermal history and lithology depend predominantly on the time that it accreted. This parameter controls the concentration of short-lived radionuclides (principally  $^{26}\text{Al}$ , which has a half-life of ~0.7 Myr) incorporated into the body

and hence the amount of radiogenic heating it experiences. Thermal evolution models assuming instantaneous accretion predict that early accreted bodies ( $\lesssim 2$  Myr after the formation of calcium-aluminum-rich inclusions [CAIs]) partially melted and differentiated into a rocky mantle and metallic core, whereas bodies that accreted even slightly later ( $\gtrsim 2$  Myr after CAI formation) remained unmelted and entirely undifferentiated (Hevey & Sanders, 2006). Combined with the common central assumption that groups of meteorites with similar chemical and isotopic signatures are samples of separate bodies, this predicted bimodality in planetesimal differentiation motivated the paradigm that chondrite and achondrite groups originate from distinct undifferentiated and differentiated bodies, respectively (Weiss & Elkins-Tanton, 2013).

Recently, the discrete nature of asteroid differentiation has been challenged by paleomagnetic measurements of CV chondrites, which argue that the postaccretional unidirectional natural remanent magnetization (NRM) carried by these meteorites is the product of magnetic fields generated by core dynamo activity (Carporzen et al., 2011; Fu et al., 2014; Gattacceca et al., 2016; Shah et al., 2017). This observation implies that the parent bodies of some chondrites were partially differentiated, consisting of a variably metamorphosed, but unmelted, chondritic crust atop a melted interior that contains an advecting metallic core (Elkins-Tanton et al., 2011). Thermal evolution models suggest that such partially differentiated bodies likely began forming when  $^{26}\text{Al}$  was abundant (i.e.,  $\lesssim 2$  Myr after CAI formation) and continued to accrete material (possibly episodically) for perhaps 0.5–4 Myr. These models also suggest that these bodies could have generated early (within the first  $\sim 5$ –15 Myr after CAI formation) magnetic fields (Bryson et al., 2019; Elkins-Tanton et al., 2011). However, the multistage and relatively poorly constrained thermal and aqueous alteration histories of CV chondrites as well as the antiquity of their NRM (likely recorded within 10 Myr of CAI formation, not long after nebula dissipation; Weiss & Elkins-Tanton, 2013) have motivated alternative hypotheses for the origin of their NRM other than core dynamo activity. These hypotheses include the early solar wind (Tarduno et al., 2017; although see Oran et al., 2018), the solar nebula (Cisowski, 1987), and/or transient impact-produced plasmas (Muxworthy et al., 2017).

A robust test of the hypothesis that some chondrites could have been magnetized by dynamo fields and that their parent bodies could have been partially differentiated would be to identify a stable NRM in a chondrite that underwent well-constrained and prolonged cooling over tens to hundreds of millions of years. This chondrite would have recorded its NRM long after nebula dissipation (only existed within the first  $<3.8$ – $4.8$  Myr; Wang et al., 2017), cooled slowly enough that quick variations in the solar wind field (timescale of days) produce a very weak time-averaged intensity ( $<3.5$  nT; Oran et al., 2018) and cooled negligibly within the extremely brief lifetime of impact-generated fields on asteroid-sized bodies ( $<10$  s; Crawford & Schultz, 2000). Compared to the CV chondrites, it is considerably less likely that this slowly cooled chondrite could have been magnetized by an external field. Instead, this chondrite is much more likely to have been magnetized by core dynamo fields, which are predicted to have been generated tens to hundreds of million years after CAI formation and for periods of possibly tens of million years (Bryson et al., 2015; Nimmo, 2009). Hence, the observation of a young and long-lived remanence in a chondrite would provide robust evidence that its parent asteroid contained a core and was therefore partially differentiated. With this motivation, we present paleomagnetic measurements of the relatively young (the measured  $^{40}\text{Ar}$ – $^{39}\text{Ar}$  ages of two Portales Valley samples are  $90 \pm 11$  and  $109 \pm 14$  Myr after CAI formation, which corresponds to the time the meteorite cooled through  $\sim 330$  and  $\sim 230$  °C, respectively; Bogard & Garrison, 2009) and slowly cooled (metallurgical cooling rate of 25 °C/Myr at  $\sim 500$  °C; Scott et al., 2014) H6 ordinary chondrite metal-silicate breccia Portales Valley (Ruzicka et al., 2005). This meteorite contains annealed microstructural evidence that it experienced an early impact when it was at a temperature  $>800$ – $1000$  °C (Rubin, 2004; Ruzicka et al., 2015), after which it remained essentially unshocked (did not experience shock pressures  $>5$  GPa) during subsequent slow cooling (Scott et al., 2014; Stöfler et al., 1991). Portales Valley was therefore above the Curie temperature of any magnetic phases found in this meteorite (Rochette et al., 2003, 2008) when it last experienced a significant impact, further ruling out the possibility that any stable NRM in Portales Valley is the produce of an impact-generated field. Portales Valley therefore provides us with an opportunity to examine the possibility that some chondrites were magnetized by late-stage magnetic fields and that some chondrite parent bodies were partially differentiated.

Although ordinary chondrites make up  $\sim 75\%$  of meteorites, they have largely evaded reliable paleomagnetic study until now because their magnetic mineralogy is dominated by magnetically unstable multidomain grains and/or strongly magnetostatically interacting assemblages (Gattacceca et al., 2014). Portales Valley is unique among ordinary chondrites as it is composed of approximately equal portions of partially melted

silicates and centimeter-sized Fe-Ni veins. These metal veins contain microstructures that formed during low-temperature recrystallization upon slow cooling (Scott et al., 2014). One component of these microstructures is the cloudy zone (CZ), a nanoscale intergrowth of islands of tetrataenite (tetragonal, chemically ordered  $\text{Fe}_{0.5}\text{Ni}_{0.5}$ ) and an Fe-rich matrix phase (Uehara et al., 2011). Tetrataenite is an extremely magnetically hard mineral (intrinsic coercivity  $>2$  T) whose [001] magnetic easy axis forms along one of the three [100] axes of the parent taenite phase (Néel et al., 1964). The presence of a magnetic field during tetrataenite ordering has been proposed to have imparted a remanence to the CZ by influencing the proportions of each of the [100] axes of the parent taenite that become the [001] magnetic easy axis of the tetrataenite (Bryson, Church, et al., 2014). The magnetization of the CZ can be studied in isolation from the bulk magnetization of a metal-rich meteorite using X-ray photoemission electron microscopy (XPEEM; Bryson, Herrero-Albillos et al., 2014). This technique provides images of the CZ magnetization from which the distribution of the easy axes among the tetrataenite islands and the properties of a magnetic field experienced by metal-rich meteorites can be estimated. XPEEM has previously been used to constrain the magnetic history of the main-group pallasites (Bryson et al., 2015; Nichols et al., 2016) and the IVA (Bryson et al., 2017), IAB (Nichols et al., 2016), and IIE (Maurel et al., 2018) iron meteorites.

Here, we apply XPEEM to the metal veins in Portales Valley with the aim of identifying whether this meteorite experienced a magnetic field when the tetrataenite islands in its CZ chemically ordered and using our observations to constrain the differentiated state of its parent body. We complement these measurements with a suite of asteroid thermal evolution models aimed at identifying whether the thermal evolution of partially differentiated bodies are consistent with measured thermal history of multiple H chondrites and the generation of a late-stage planetary magnetic field through dynamo activity.

## 2. Materials and Methods

### 2.1. General Petrographic Description

Portales Valley is a unique chondrite that consists of partially melted silicates and centimeter-sized Fe-Ni veins. Both of these components bear strong elemental and isotopic similarities to the H chondrites, indicating that the protolith of Portales Valley was H chondrite material (Ruzicka et al., 2005). However, Portales Valley differs from other H chondrites because it reached higher peak metamorphic temperatures (940–1150 °C; Ruzicka et al., 2005). Portales Valley contains annealed evidence of an early shock event (likely S3–S6; Rubin, 2004) that occurred when the meteorite was at high temperature ( $>800$ – $1000$  °C; Ruzicka et al., 2015). This observation led Ruzicka et al. (2005) to propose that the metal veins in this meteorite could have formed when stresses from this impact separated molten metal from partially molten silicates. There is no requirement from geochemical observations for the addition of a significant amount of heat to the meteorite during this impact, meaning that it is possible that the partial melting of Portales Valley could have been the result of endogenic heat from  $^{26}\text{Al}$  decay (Ruzicka et al., 2005). If so, the petrography of Portales Valley would be evidence for the partial differentiation of its parent body. However, it is also possible that this impact added some heat to this meteorite, which, on top of the endogenic heat, could have caused its partial melting.

### 2.2. Magnetic Mineralogy

A series of microstructures form in meteoritic metal during slow cooling. These microstructures start forming on cooling through  $\sim 900$  °C when lamellae of the Ni-poor phase kamacite nucleate and grow out of the parent taenite phase. Ni is rejected from these lamellae as they grow, introducing a Ni gradient in the adjacent taenite that varies from  $\sim 50\%$  Ni immediately adjacent to the kamacite lamellae down to the bulk metal Ni concentration ( $\sim 7\%$  Ni in Portales Valley; Ruzicka et al., 2005) over 10–20  $\mu\text{m}$  (Uehara et al., 2011). The gradient of this Ni zoning indicates that Portales Valley cooled at 25 °C/Myr through  $\sim 500$  °C (Scott et al., 2014).

On cooling below 320 °C, pure tetrataenite forms as a rim adjacent to the kamacite lamellae at Ni compositions between  $\sim 50\%$  and 42% (Goldstein et al., 2009). This rim forms from the same parent taenite as that of the CZ and contains large ( $>1$   $\mu\text{m}$ ) twin domains, each consisting of one of the three different possible tetrataenite easy axes (Bryson, Herrero-Albillos et al., 2014). The CZ forms adjacent to the rim at Ni concentrations between  $\sim 42\%$  and  $<25\%$  via spinodal decomposition (Maurel et al., 2019). This process starts at  $\sim 400$  °C and decreases in temperature as the Ni concentration decreases (Uehara et al., 2011). The islands that form at higher Ni concentration (those closer to the rim) therefore formed at higher temperatures and earlier times than those that formed at lower Ni concentration (those further from the rim). This Ni concen-

tration gradient also leads to a decrease in island size across the width of the CZ (Maurel et al., 2019). The similarity in the diameter of the largest islands in the CZ in both the silicate-rich portion ( $109 \pm 5.2$  nm) and the metal veins ( $106.3 \pm 7.1$  nm) in Portales Valley indicate that these two constituents cooled at a single rate at temperatures below  $\sim 400$  °C (Scott et al., 2014). The weighted average diameter of the CZ islands in both constituents of the Portales Valley is 108 nm (Scott et al., 2014).

Islands that form at temperatures between 400 and 320 °C do so as taenite and order to form tetrataenite as the meteorite cools through 320 °C (Einsle et al., 2018). Recent micromagnetic modeling (Einsle et al., 2018) demonstrates that these islands recorded a new chemical transformation remanent magnetization during ordering and that this remanence is independent of the magnetic state of the parent taenite. Consequently, all the islands that had formed before a meteorite reached 320 °C will have recorded a new remanence during ordering at the same time. The remanence across the width of the CZ is therefore unlikely to reflect a time-resolved record of dynamo activity over millions of years as previously thought (Bryson et al., 2015; Nichols et al., 2016, 2018). Prior to this transition, these larger islands adopted vortex domain states, meaning they experienced relatively weak magnetostatic interaction fields (Einsle et al., 2018). Finer islands that formed at temperatures  $< 320$  °C likely did so as single-domain tetrataenite, causing them to experience more intense interaction fields that possibly strongly favored one easy axis among these islands (Bryson, Church, et al., 2014; Einsle et al., 2018). We intentionally do not analyze these fine islands due to these intense interactions. The tetrataenite ordering temperature is similar to the  $^{40}\text{Ar}$ - $^{39}\text{Ar}$  closure temperature of Portales Valley ( $\sim 330$ – $230$  °C; Bogard & Garrison, 2009), indicating that the CZ in this meteorite recorded its NRM  $\sim 100$  Myr after CAI formation. The measured rate of tetrataenite disordering at 320 °C is certainly  $\gg 11$  days and probably  $\sim 30$ – $300$  years (Dos Santos et al., 2015). These disordering timescales indicate that tetrataenite ordering lasted for at least this period and was possibly longer as the rate of change in order parameter in binary alloys is often slower during ordering than disordering (e.g., Morris et al., 1974). Remanence acquisition therefore occurred over a long time period relative to the duration of impact-generated fields (Crawford & Schultz, 2000) and the rate of change of the solar wind field (Oran et al., 2018).

The volume of the islands at the time that they ordered has been suggested to have played a significant role in the proportions of each of the possible easy axes that form among the CZ for a given field intensity (Berndt, et al., 2016; Bryson, Church, et al., 2014). Through modeling spinodal decomposition, Maurel et al. (2019) found that islands had a radius of  $\sim 78\%$  of their present-day value when the CZ cooled through 320 °C for bulk CZ Ni concentrations of  $\sim 40\%$ . This value is far larger than the thermal blocking volume of tetrataenite (which corresponds to a radius of 4 nm), greatly reducing the number of islands required for estimates of the paleofield properties at 95% confidence from previous estimates of  $\sim 100,000$  (Berndt et al., 2016, see section 4.1). We present paleofield properties using an island volume corresponding to a radius of 42 nm (78% of the weighted average present-day radius of the largest islands). The island size decreases across the CZ; however, the rate at which this occurs in our specific sample depends on the relative orientations of the surface we imaged and the kamacite lamellae. Regardless, our adopted radius is likely an overestimate of the average island size across the regions we analyzed, meaning that our paleointensity estimates are lower limits.

### 2.3. X-ray Photoelectron Emission Microscopy

We obtained a sample of Portales Valley from the Natural History Museum, London (sample number BM 1999.M.50) that contained both the silicate- and metal-rich portions of this meteorite. We captured XPEEM images at multiple locations along two separate CZ-bearing interfaces (termed interface A and B, separated by  $\sim 6$  mm, Figure 1) at beamline 11.0.1 at the Advanced Light Source, Lawrence Berkeley National Laboratory. We imaged interface A in August 2015 during “two-bunch” synchrotron operation and interface B in February 2016 during normal synchrotron operation. Prior to XPEEM measurements, we sputtered our subsample with Ar ions (8 hr at 1.2 keV, followed by 8 hr at 0.8 keV, and finally 1 hr at 0.6 keV) under ultra-high vacuum at the beamline to ensure the surface was clean and to remove an  $\sim 80$ -nm thick magnetically soft layer that was introduced during polishing (Bryson, Church, et al., 2014; Bryson, Herrero-Albillos, et al., 2014).

The magnetic contrast in our XPEEM images is provided by X-ray magnetic circular dichroism (XMCD), whereby the efficiency of electron ejection from the sample's surface by circularly polarized X-rays depends on the relative orientation of the local magnetic moment and the X-ray beam (Bryson, Herrero-Albillos et al., 2014). Once ejected from the sample surface, the electrons pass through a series of focusing lenses to generate a map of the local projection of the surface magnetic moment onto the X-ray beam direction. This



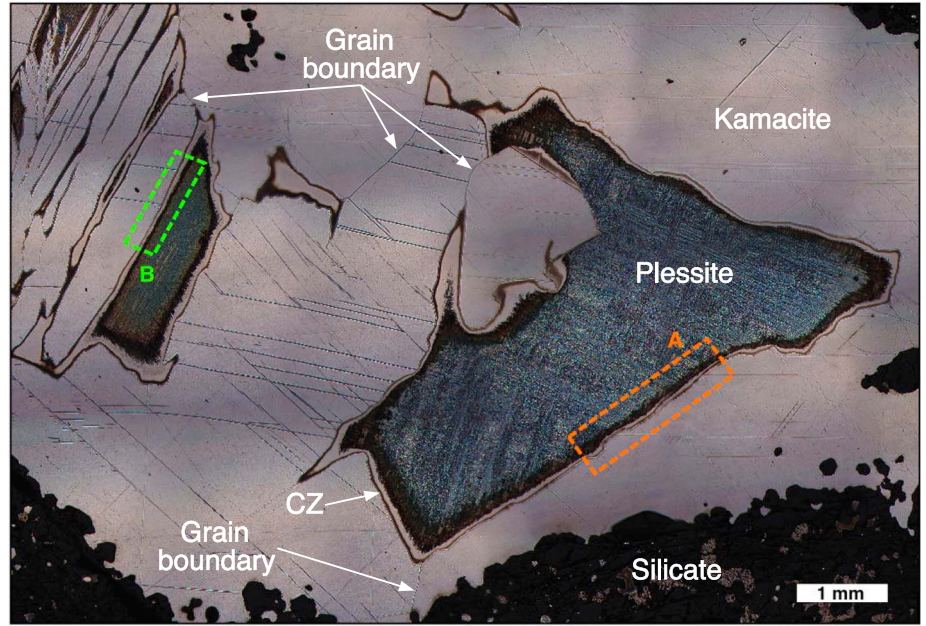


**Figure 1.** Optical microscopy image of the interfaces we measured in our sample of Portales Valley. The sample had been etched with 2% nital for 20 s prior to imaging to highlight the microstructures. The area of the cloudy zone (CZ) along interfaces A and B that we measured are labeled with colored boxes.

technique probes the magnetization of the top ~5 nm of the sample. The XPEEM intensity,  $I$ , is calculated as the difference between images captured with right,  $I_R$ , and left,  $I_L$ , circular polarized X-rays, divided by the sum of these images:

$$I = \frac{I_R - I_L}{I_R + I_L} \quad (1)$$

We present  $I$  rather than  $I_R$  or  $I_L$  because  $I$  is independent of the sample's composition and minimizes effects of fluctuations in beam intensity. Blue and red signals in our XPEEM images correspond to positive and negative projections of the local magnetic moment onto the X-ray beam direction, respectively. We adopted a new experimental procedure during both beamtimes where we imaged each location at three orientations of the sample with respect to the X-ray beam. This methodology allowed us for the first time to directly estimate the direction and intensity of the ancient field experienced by the CZ, improving upon single field component and paleointensity lower limits presented in previous studies that imaged samples at only one sample orientation with respect to the X-ray beam (Bryson et al., 2015, 2017; Nichols et al., 2016, 2018). We achieved this by rotating the sample by ~120° around an axis perpendicular to its surface between measurements. Assuming the average proportion of each easy axis among a large number of CZ islands is dominated by the energy of that direction in a magnetic field with a given orientation and thermal fluctuations, the XMCD signal averaged over a region of the CZ,  $I_A$ , can be expressed as

$$I_A = \frac{I_x e^{\frac{M_s V B_x}{k_B T_0}} + I_{-x} e^{-\frac{M_s V B_x}{k_B T_0}} + I_y e^{\frac{M_s V B_y}{k_B T_0}} + I_{-y} e^{-\frac{M_s V B_y}{k_B T_0}} + I_z e^{\frac{M_s V B_z}{k_B T_0}} + I_{-z} e^{-\frac{M_s V B_z}{k_B T_0}}}{e^{\frac{M_s V B_x}{k_B T_0}} + e^{-\frac{M_s V B_x}{k_B T_0}} + e^{\frac{M_s V B_y}{k_B T_0}} + e^{-\frac{M_s V B_y}{k_B T_0}} + e^{\frac{M_s V B_z}{k_B T_0}} + e^{-\frac{M_s V B_z}{k_B T_0}}} \quad (2)$$

where  $x$ ,  $y$ , and  $z$  are the three possible tetraenite easy axes;  $I_x$ ,  $I_{-x}$ ,  $I_y$ ,  $I_{-y}$ ,  $I_z$ , and  $I_{-z}$  are the XMCD intensities of the three pairs of possible tetraenite magnetization directions extracted from the tetraenite rim corresponding to the easy axes;  $B_x$ ,  $B_y$ , and  $B_z$  are the components of the paleofield intensity along the easy axes;  $T_0$  is the tetraenite ordering temperature (320 °C);  $V$  is the mean volume of an island at  $T_0$ ;  $M_s$  is the saturation magnetization of tetraenite at  $T_0$  ( $1.12 \times 10^6$  A/m); and  $k_B$  is Boltzmann's constant (Bryson, Church, et al., 2014). This expression assumes that islands are magnetically noninteracting; the errors and

uncertainties introduced by this assumption are discussed in section 4.1. The domains in the tetrataenite rim are typically  $>1 \mu\text{m}$  along their longest dimension and display uniform values of  $I_x$ ,  $I_{-x}$ ,  $I_y$ ,  $I_{-y}$ ,  $I_z$ , and  $I_{-z}$  providing a means of reliably extracting these values from our XPEEM images (Figure S1). We extracted these values from as many images as possible (the tetrataenite rims in some locations did not contain all six of these values), from which we calculated an average value of each of these intensities and used these averages values to recover paleointensities. For typical values of  $V$  ( $\sim 5 \times 10^{-21}$  to  $5 \times 10^{-24} \text{ m}^3$ ) and  $B_x$ ,  $B_y$ , and  $B_z$  ( $\sim 1\text{--}100 \mu\text{T}$ ),  $I_A$  can be approximated as

$$I_A \approx \frac{M_s V}{6k_B T_0} \left( (I_{-x} - I_x) B_x + (I_{-y} - I_y) B_y + (I_{-z} - I_z) B_z \right) + \frac{1}{6} (I_x + I_{-x} + I_y + I_{-y} + I_z + I_{-z}) \quad (3)$$

Rotating a sample about an axis perpendicular to the surface changes the orientation of the X-ray beam with respect to the tetrataenite easy axes such that the values of  $I_x$ ,  $I_{-x}$ ,  $I_y$ ,  $I_{-y}$ ,  $I_z$ , and  $I_{-z}$  all change, while the paleofield components  $B_x$ ,  $B_y$ , and  $B_z$  remain constant by definition. In this second rotation, the value of the average XMCD intensity,  $I'_A$ , can be approximated as

$$I'_A \approx \frac{M_s V}{6k_B T_0} \left( (I'_{-x} - I'_x) B_x + (I'_{-y} - I'_y) B_y + (I'_{-z} - I'_z) B_z \right) + \frac{1}{6} (I'_x + I'_{-x} + I'_y + I'_{-y} + I'_z + I'_{-z}) \quad (4)$$

where  $I'_x$ ,  $I'_{-x}$ ,  $I'_y$ ,  $I'_{-y}$ ,  $I'_z$ , and  $I'_{-z}$  are the XMCD intensities extracted from the tetrataenite rim in this second rotation from the same domains as in the previous rotation. Finally, for a third sample orientation, the third average XMCD intensity,  $I''_A$ , can be approximated as

$$I''_A \approx \frac{M_s V}{6k_B T_0} \left( (I''_{-x} - I''_x) B_x + (I''_{-y} - I''_y) B_y + (I''_{-z} - I''_z) B_z \right) + \frac{1}{6} (I''_x + I''_{-x} + I''_y + I''_{-y} + I''_z + I''_{-z}) \quad (5)$$

where  $I''_x$ ,  $I''_{-x}$ ,  $I''_y$ ,  $I''_{-y}$ ,  $I''_z$ , and  $I''_{-z}$  are the XMCD intensities extracted from the tetrataenite rim in this third rotation. We calculated  $B_x$ ,  $B_y$ , and  $B_z$  by solving equations (3)–(5) simultaneously using  $I_A$ ,  $I'_A$ ,  $I''_A$  values extracted from one large region ( $\sim 9 \mu\text{m} \times \sim 2 \mu\text{m}$ ) in the CZ starting adjacent to the tetrataenite rim at each of our locations (Figure 2). We analyzed regions of this size to incorporate as many islands as possible that do not display an XMCD signal indicating that their remanence has clearly been influenced by interactions that favor one easy axis. Furthermore, as discussed in section 4.1, magnetostatic interactions likely influenced the CZ remanence, so analyzing wide regions of the CZ that contain islands further from the rim that are separated by relatively large distances compared to their size likely reduces the impact of these interactions on our recovered paleofield properties.

We assessed the quality of all of the images we captured and disregarded any that contained detrimental beam drift or sample tilting that defocused or introduced a background intensity ramp to the images. We accepted 18 of the locations we imaged along interface A and 19 locations along interface B.

As mentioned earlier, the rate of island size decrease across the CZ along the interfaces we measured depends on the orientation of our sample surface and the kamacite lamellae. If the lamellae and surface are nearly parallel, the island size is essentially constant across the width of the CZ we analyzed. On the other hand, if the lamellae and surface are perpendicular, previous studies (Bryson, Church, et al., 2014; Einsle et al., 2018; Uehara et al., 2011) suggest that islands at a distance of  $\sim 2 \mu\text{m}$  from the tetrataenite rim are  $\sim 0.5$  times the size of those next to the rim (i.e., radius of 21 nm when they recorded a remanence in Portales Valley). Assuming that the island radius is 42 nm across the width of the CZ that we analyzed and that the islands occupy 90% of the CZ (Maurel et al., 2019) provides an estimate on the lower limit of the number of islands we imaged along each interface of  $\sim 47,000$ . Assuming an island radius of 21 nm across the width of the CZ provides an estimate on the upper limit of the number of islands we imaged along each interface of  $\sim 190,000$  (see section 4.1).

#### 2.4. Asteroid Thermal Modeling

The thermal evolution of the H chondrite parent body has been constrained by a variety of thermochronometers and cooling rate measurements on multiple H chondrites. Asteroid thermal evolution models have demonstrated that undifferentiated but variably metamorphosed bodies are broadly compatible with these data (Henke et al., 2013; Monnereau et al., 2013), although the existence of an onion-shell thermal structure throughout the entire cooling history of the H chondrite parent body is debated (Blackburn et al., 2017; Scott et al., 2014). A key test of the hypothesis that the H chondrite body was partially differentiated is that the



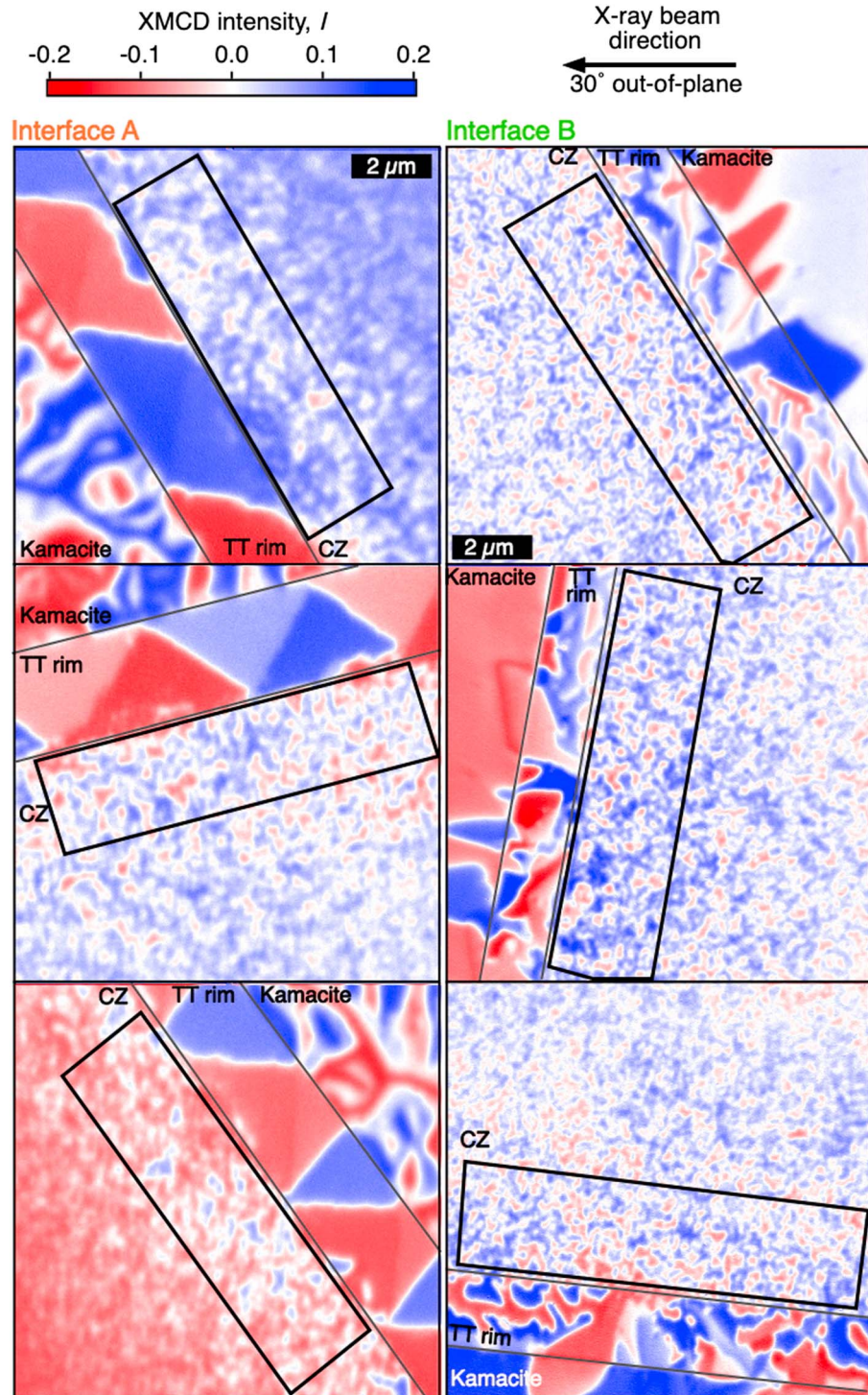


**Figure 2.** XPEEM images of the cloudy zone (CZ) in our sample of Portales Valley. These images are representative of the images we captured along interface A (left panels) and B (right panels). Images were acquired at three sample rotations (top, middle, and bottom rows). The color depicts the XMCD intensity, with blue and red signals corresponding to positive and negative projections along the X-ray beam direction (top right, constant across all panels), respectively. The paleofield properties were calculated from the average XMCD intensity extracted from the regions within the black boxes in each panel. The scale bars for all images from interfaces A and B are included in the top panel for each interface. The kamacite, tetraenaite (TT) rim, and CZ are separated by gray lines. XPEEM = X-ray photoemission electron microscopy; XMCD = X-ray magnetic circular dichroism.

thermal evolution of such a body should be compatible with the available thermochronometry and cooling rate data. To assess whether this could be the case, we performed one-dimensional models of the thermal evolution of a spherical body that accreted in two discrete events (Bryson et al., 2019). The mathematical description of our model and values of the parameters we adopted are detailed by Bryson et al. (2019). We model the thermal evolution of a body that forms through instantaneous accretion of material with thermal diffusivity  $\kappa = 9 \times 10^{-7} \text{ m}^2 \text{ s}^{-1}$  (Opeil et al., 2012) at time  $t_1$  with radius  $r_1$  that is covered at a later time,  $t_2$ , by a large number of cold chondrules that increase its radius to  $r_2$  (Elkins-Tanton et al., 2011). This process has been proposed as a likely growth mechanism for asteroids with radii  $>100 \text{ km}$  (Johansen et al., 2015). The initial body forms early enough that it can differentiate and form a core, and the later addition of chondrules to its surface could result in a partially differentiated body if some of these chondrules survive metamorphism without melting. Our model is idealized and our intention is not to identify the exact properties, thermal evolution or accretional history of the H chondrite parent asteroid but simply to assess the feasibility that the modeled thermal evolutions of partially differentiated and undifferentiated bodies are similarly consistent with the measured thermal evolutions of multiple H chondrites. If we demonstrate that our accretion scenarios are compatible with measured ages and cooling rates, partial differentiation should be considered as one potential model for the H chondrite parent body given that there are innumerable other possible gradual accretion scenarios with different accretion rates and durations that might also produce these bodies (e.g., Lichtenberg et al., 2018).

We conducted 2,000 simulations with randomly chosen combinations of  $r_1$ ,  $t_1$ ,  $r_2$ , and  $t_2$ . Values of  $t_1$  were chosen at random from a uniform distribution spanning 0.0–2.0 Myr after CAI formation, corresponding to the period when the accreting material contained enough  $^{26}\text{Al}$  to partially melt. Values of  $t_2$  were chosen between 2.0 and 4.5 Myr after CAI formation, corresponding to the period when the material added in the second event was variably heated but not melted by  $^{26}\text{Al}$  decay. Values of  $r_1$  were chosen between 20 and 500 km and values of  $r_2$  were chosen between  $r_1 + 1$  and 500 km. These radii ranges incorporate the smallest bodies that could retain enough radiogenic heat to cause differentiation (Hevey & Sanders, 2006) and extend up to the size of the largest asteroids in the asteroid belt at the present day.

We judged the quality of each random parameter combination by comparing the thermal evolutions at depth throughout the added chondritic material to the measured ages of multiple H chondrites that have been dated using multiple geochronological systems with different closure temperatures (Amelin et al., 2005; Bli-nova et al., 2007; Bouvier et al., 2007; Kleine et al., 2008; Trierloff et al., 2003). We considered the  $^{182}\text{Hf}$ – $^{182}\text{W}$ ,  $^{207}\text{Pb}$ – $^{206}\text{Pb}$  in silicates,  $^{207}\text{Pb}$ – $^{206}\text{Pb}$  in phosphates,  $^{40}\text{Ar}$ – $^{39}\text{Ar}$  and  $^{244}\text{Pu}$ -fission track ages measured from the Richardton, Kernouvé, and Estacado H chondrites (Table S1 in the supporting information), and the  $^{207}\text{Pb}$ – $^{206}\text{Pb}$  in phosphates,  $^{40}\text{Ar}$ – $^{39}\text{Ar}$ , and  $^{244}\text{Pu}$ -fission track ages measured from Ste. Marguerite. We did not consider the  $^{182}\text{Hf}$ – $^{182}\text{W}$  and  $^{207}\text{Pb}$ – $^{206}\text{Pb}$  in silicates ages measured from Ste. Marguerite as it has previously been argued that the peak metamorphic temperature experienced by this meteorite was insufficient to reset these geochronological systems so they date chondrule formation rather than parent body metamorphism (Henke et al., 2013). Furthermore, we also considered the measured radiometric ages of the Forest Vale, Nadiabondi, Allegan, Mt. Browne, and Guareña H chondrites (Table S1 in the supporting information). However, due to the sparsity and/or uncertainty in their ages, these meteorites do not additionally constrain the parent body properties or thermal evolution and consequently are only discussed further in the supporting information.

For a given parameter combination, the depth within the chondritic layer that produced the thermal evolution that closest matched the closure temperatures at the measured ages of a given meteorite is assigned as the depth of that meteorite. We calculated the closeness of the thermal evolution at each depth,  $C$ , as the sum of the square of the temperature difference between the model thermal evolutions,  $T_{\text{calc}}$ , and the closure temperatures,  $T_{\text{ct}}$ , at the measured ages for a given meteorite:

$$C = \Sigma[(T_{\text{ct}} - T_{\text{calc}})^2] \quad (6)$$

We present a total average residual value,  $R$ , calculated as the square root of the sum of the minimum closeness values,  $C_{\text{min}}$ , for all four meteorites divided by the total number of measured ages,  $n$ , from all four meteorites:

$$R = \frac{\sqrt{\Sigma C_{\text{min}}}}{n} \quad (7)$$



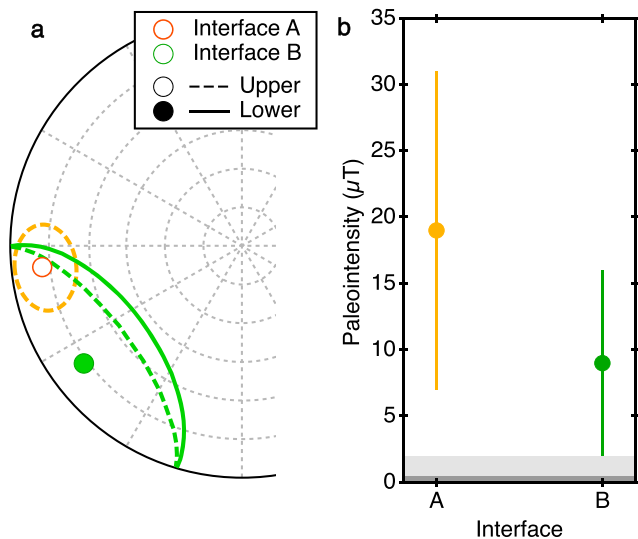


**Figure 3.** Ancient field properties recovered from XPEEM images of Portales Valley. (a) Stereographic projection showing the orientations of the average paleofield recovered from both interfaces studied. The 95% confidence interval along each interface calculated from the scatter in the recovered paleodirections from the different locations along each interface are included as the ellipses. Filled points and solid lines represent the lower hemisphere of the stereoplot and open points and dashed lines represent the upper hemisphere. (b) Lower limits on the paleointensities recovered from both interfaces. The total 95% uncertainties are depicted by the error bars (see section 4.1). The calculated 95% confidence limits on the possible paleointensities that could be recovered from the absence of a field taken from Figure 3 are included as a dark gray bar for 47,000 islands with a radius of 42 nm and a light gray bar for 190,000 islands with a radius of 21 nm. Our recovered paleointensities are outside of these ranges, indicating that the remanence we measure in Portales Valley is unlikely to correspond to the absence of a field. XPEEM = X-ray photoemission electron microscopy.

This value is a measure of the overall fit quality for a given parameter combination, with lower values corresponding to better fits. The error bars on the data points correspond to 95% confidence on the ages and realistic estimates of the uncertainty in the closure temperatures (Henke et al., 2013; Kleine et al., 2008; Monnereau et al., 2013). These ranges create rectangular regions in age-closure temperature space through which acceptable simulated thermal evolutions of each meteorite would ideally pass. The total number of these rectangular regions from Ste. Marguerite, Richardton, Kernouvé, and Estacado that are missed by their simulated thermal evolution curve is termed the score,  $S$ , with lower values corresponding to better fits to the measured thermal evolutions.

We also conducted thermal evolution models of undifferentiated bodies. These models allowed us to compare the qualities of the fits recovered from our partially differentiated model directly with those recovered from equivalent models of undifferentiated bodies. The parameters and underlying mathematical description of the two models are identical (Bryson et al., 2019). The undifferentiated models simply involved the production and conduction of radiogenic heat from  $^{26}\text{Al}$  decay. We conducted 2,000 of these models with random combinations of accretion time,  $t$ , ranging between 2.0 and 4.5 Myr after CAI formation and radius,  $r$ , ranging between 20 and 500 km. We calculated  $R$  and  $S$  values for these models through the same method as the partially differentiated model and compared them with those calculated in the partially differentiated model.

### 3. Results

#### 3.1. X-ray Photoemission Electron Microscopy

Representative XPEEM images of the CZ along interface A and B at all three sample rotations with respect to the X-ray beam are shown in Figure 2. We extracted  $I_A$ ,  $I'_A$ , and  $I''_A$  values from one large region ( $\sim 9 \times 2 \mu\text{m}$ , black boxes) of the CZ at all locations we analyzed. The paleodirections we recover from these values are within error of each other along each interface accounting for the scatter in  $I_A$ ,  $I'_A$ , and  $I''_A$  values from location to location (Figure 3a). The recovered paleointensities are  $19 \pm 12 \mu\text{T}$  for interface A and  $9 \pm 7 \mu\text{T}$  for interface B (total 95% error; Figure 3b), also within error of each other. The errors and uncertainties on these values are discussed in section 4.1. These values are lower limits given the likely decrease in island size across the CZ regions we analyzed.

Although our recovered paleointensities are  $>0 \mu\text{T}$  to 95% confidence, we made certain that our measured remanences could not reflect the absence of a field by calculating the range of paleointensities we would expect for equal probabilities that an island adopts any one of the six possible magnetization directions (expected magnetization configuration in the absence of a field) over 47,000 islands with a radius of 42 nm and 190,000 islands with a radius of 21 nm (encompassing the range of island sizes and numbers that we possibly analyzed). The mathematical details of this method are described by Bryson et al. (2017). We repeated this process 10,000 times, finding that 95% of these calculations produce paleointensities  $\leq 0.5$  and  $\leq 2.0 \mu\text{T}$  for 42 and 21 nm islands, respectively (Figure 4). Regardless of the island size we adopt, our recovered paleointensities are greater than these limits, allowing us to exclude with 95% confidence the possibility that our XPEEM images correspond to the absence of a field.

Although our recovered paleointensities are  $>0 \mu\text{T}$  to 95% confidence, we made certain that our measured remanences could not reflect the absence of a field by calculating the range of paleointensities we would expect for equal probabilities that an island adopts any one of the six possible magnetization directions (expected magnetization configuration in the absence of a field) over 47,000 islands with a radius of 42 nm and 190,000 islands with a radius of 21 nm (encompassing the range of island sizes and numbers that we possibly analyzed). The mathematical details of this method are described by Bryson et al. (2017). We repeated this process 10,000 times, finding that 95% of these calculations produce paleointensities  $\leq 0.5$  and  $\leq 2.0 \mu\text{T}$  for 42 and 21 nm islands, respectively (Figure 4). Regardless of the island size we adopt, our recovered paleointensities are greater than these limits, allowing us to exclude with 95% confidence the possibility that our XPEEM images correspond to the absence of a field.

The recovered paleodirections have 95% confidence ellipses of  $11^\circ$  and  $37^\circ$  along interfaces A and B, respectively, taking into account the measurement uncertainty (scatter in average XMCD values extracted from location to location along an interface). These values are shown in Figure 3a as the 95% confidence ellipses. Our analysis procedure provides the projection of the field direction along each of the three possible tetraenite easy axis directions along a given interface. Interface A and B are located in separate grains (Figure 1) with different crystallographic orientations, so we had to map the recovered directions onto the

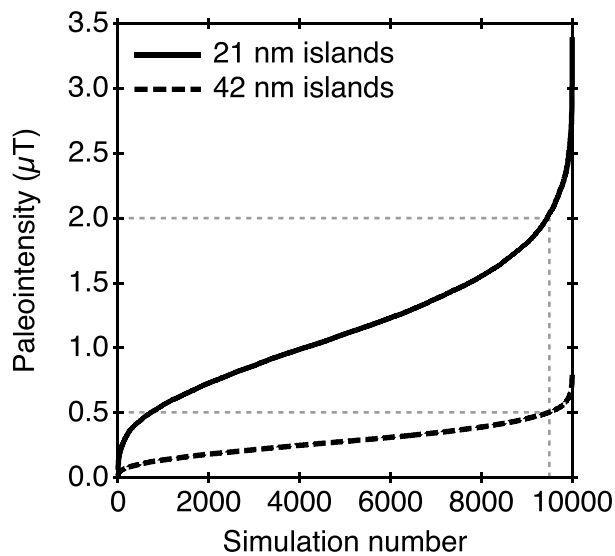


**Figure 4.** Cumulative probability distribution showing the paleointensities of 10,000 simulated CZs with equal probability that its islands adopt any one of the six possible magnetization directions, corresponding to the magnetic configuration expected in the absence of an external magnetic field (see Bryson et al., 2017). We conducted simulations with 47,000 islands with radii of 42 nm and 190,000 islands with radii of 21 nm, encompassing the possible range of island sizes and numbers we analyzed. The vertical dashed lines marks 95% of the simulations, suggesting that recovered paleointensities  $>0.5 \mu\text{T}$  and  $>2 \mu\text{T}$  for islands with radii of 42 and 21 nm, respectively, are inconsistent with zero field magnetization at the 95% confidence level.

same directional framework to mutually orient our recovered directions and assess whether they are unidirectional. We accomplished this by first estimating the directions of the three possible easy axes along each interface relative to the bounding box of the images from the values of the XMCD intensity of the domains in the tetraenaite rim at each sample rotation. We then generated the rotation matrix relating these axes and applied it to the directions recovered from the different CZ regions along each interface. The orientations we recovered from the XMCD intensities in the rim were not orthogonal (most likely because of slight moment relaxation), introducing an error in the recovered paleodirections (see supporting information). The 95% confidence error associated with this uncertainty is  $16^\circ$  and  $34^\circ$  along interfaces A and B, respectively, which is similar to the 95% confidence angle calculated from the measurement uncertainty.

The paleodirections we recover are unidirectional, and the paleointensities we recover are greater than zero, indicating that Portales Valley recorded a spatially uniform field over a relatively long time period (likely tens to hundreds of years) at  $\sim 100$  Myr after CAI formation.

### 3.2. Asteroid Thermal Modeling

A summary of the results of our partially differentiated asteroid thermal evolution models is shown in Figure 5. Our models demonstrate that the late accretion of cold chondrules to the surface of differentiated bodies can result in the addition of an undifferentiated layer on these bodies, producing partially differentiated bodies (Figure 5b). We defined that a random parameter combination produced an acceptable fit to the measured ages if  $R \leq 27^\circ\text{C}$ , which corresponds to 95% of parameter combinations with  $S \leq 6$  (Figure 5c). We find that wide ranges of  $r_1$ ,  $t_1$ , and  $r_2$  are capable of producing acceptable fits to the measured H chondrite

ages (Figures 5a, 5d, and 5e) and measured cooling rates (Figure 6) of multiple H chondrites. The primary parameter that controls the values of  $R$  and  $S$  is  $t_2$ , which produces acceptable values of these parameters between 2.3 and 2.5 Myr after CAI formation (Figures 5d and 5e). The fit quality is also controlled to a lesser extent by the thickness of the added chondritic layer ( $r_2 - r_1$ ). The relatively short duration of the period that produces acceptable fits stems from exponential changes in the amount of heat generated by the decay of  $^{26}\text{Al}$  associated with small changes in  $t_2$ . Any difference in the values of  $t_2$  that produce the best fits in our models and the accretion times recovered from previous models of undifferentiated bodies (Doyle et al., 2015; Henke et al., 2013; Kleine et al., 2008; Monnereau et al., 2013) originates from the different values of the initial concentration of  $^{26}\text{Al}$  in the chondritic material, the adopted heat capacity of the material in the models and the additional heat supplied to the chondritic layer from the initial body. We achieved our best fit ( $R = 14.5^\circ\text{C}$ ,  $S = 5$ ) for  $r_1 = 65$  km,  $t_1 = 0.6$  Myr after CAI formation,  $r_2 = 178$  km and  $t_2 = 2.45$  Myr after CAI formation (Figure 5a). Our modeled cooling rates at  $500^\circ\text{C}$  for the recovered depth of Richardton ( $19.7^\circ\text{C/Myr}$ ), Kernouvé ( $7.3^\circ\text{C/Myr}$ ), and Estacado ( $5.7^\circ\text{C/Myr}$ ) are similar to measured values ( $20^\circ\text{C/Myr}$  for Richardton and  $10^\circ\text{C/Myr}$  for Kernouvé and Estacado), while our modeled cooling rate of Ste. Marguerite ( $46.9^\circ\text{C/Myr}$ ) is significantly slower than the measured cooling rate ( $>10,000^\circ\text{C/Myr}$ ; Scott et al., 2014). In fact, this measured rate is far quicker than that achieved in any of our models, indicating that it is likely due to a nonideal process not included in our model (e.g., impacts) that could excavate material from depth and allow it to suddenly cool uncharacteristically quickly.

A summary of the results of our undifferentiated asteroid thermal models is shown in Figure 7. We found that the parameters that produce acceptable fits in our partially differentiated model also produce acceptable fits in our undifferentiated model (Figures 7a–7c). Again, the quality of the fit depends primarily on the time of chondrule accretion and to a lesser extent the thickness of the chondritic layer (which in this model is the radius of the body). The modeled cooling rates are similar to those recovered from the partially differentiated body ( $19.5^\circ\text{C/Myr}$ ,  $8.7^\circ\text{C/Myr}$ , and  $7.5^\circ\text{C/Myr}$  for Richardton, Kernouvé and Estacado, respectively; the recovered depth of Ste. Marguerite did not reach  $500^\circ\text{C}$  in this model). Our undifferentiated body produced marginally better fits (our best fit produces  $R = 12.7^\circ\text{C}$  and  $S = 2$  for  $r = 140$  km,  $t = 2.47$  Myr

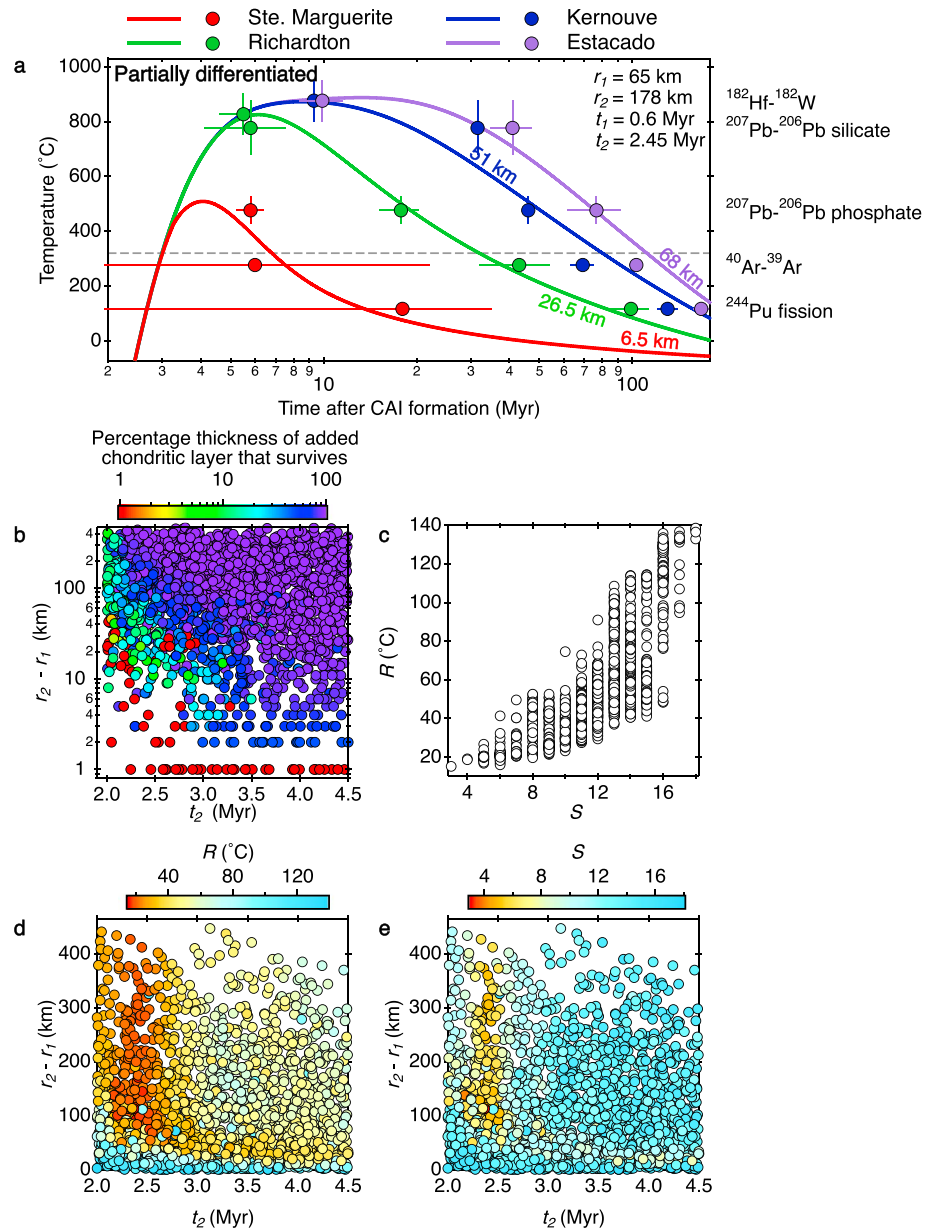


**Figure 5.** Thermal modeling of a partially differentiated H chondrite planetesimal. (a) Measured ages for four well-dated H chondrites (points) and modeled thermal evolutions (solid lines) for a body with parameters that produced the lowest  $R$  value in this model ( $r_1 = 65$  km,  $r_2 = 178$  km,  $t_1 = 0.6$  Myr after CAI formation and  $t_2 = 2.45$  Myr after CAI formation). The depth of each of the modeled thermal evolutions is included next to each curve. The parameters in this model produce  $S = 5$  and an average total residual value of  $R = 14.5$   $^{\circ}\text{C}$ . The geochronological systems are listed on the right of the figure. The horizontal dashed line depicts the tetraenaite ordering temperature. (b) All combinations of  $r_2 - r_1$  and  $t_2$  showing the proportion of the added chondritic layer that survives metamorphism without melting. (c) Plot of the two fit quality metrics. 95% of models with  $S \leq 6$  have  $R \leq 27$   $^{\circ}\text{C}$ . (d) All combinations of  $r_2 - r_1$  and  $t_2$  color coded by their  $R$  value. (e) All combinations of  $r_2 - r_1$  and  $t_2$  color coded by their  $S$  value. Lower values of  $R$  and  $S$  correspond to better fits. CAI = calcium-aluminum-rich inclusion.

after CAI formation) than our partially differentiated model due to the slightly prolonged cooling at later times in our partially differentiated bodies due to their larger size and the gradual conduction of heat from the interior of the body. In reality, it is possible that the later stages of the thermal evolution of a meteorite could have been effected by changes in cooling rates caused by processes not included in our model, such as regolith production and impacts (Warren, 2011). Importantly, the differences in  $R$  and  $S$  between our partially differentiated and undifferentiated models for similar values of  $t_2$  and thickness of chondritic layers are



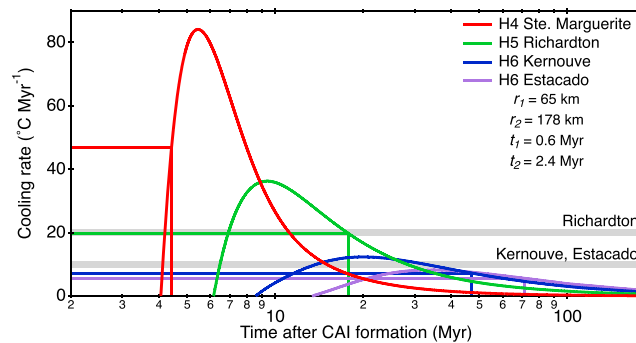


**Figure 6.** Calculated cooling rate evolution from the curves in Figure 4a. Measured metallographic cooling rates correspond to the cooling rate of a meteorite as it cooled through  $\sim 500^\circ\text{C}$  and are depicted by horizontal gray bars (Scott et al., 2014). The time that each meteorite reached this temperature is depicted by the colored vertical lines. The corresponding cooling rate at this time is depicted by the colored horizontal lines. In our model, the peak metamorphic temperature of Ste. Marguerite only just exceeded  $500^\circ\text{C}$ , so this depth cooled through  $500^\circ\text{C}$  while its cooling rate was still increasing. The experimental cooling rate of Ste. Marguerite is  $\sim 10,000^\circ\text{C/Myr}$ , which is far faster than any cooling rate achieved in our models, so is likely due to a nonideal effects not included in our models (e.g., impacts). CAI = calcium-aluminum-rich inclusion.

very small compared to the variation in  $R$  and  $S$  for different parameter combinations within either model. Furthermore, models of both types of body are capable of readily producing acceptable fits of equally good quality for a number of parameter combinations. Therefore, the measured ages and cooling rates of multiple H chondrites equally support an undifferentiated and partially differentiated H chondrite parent body.

The proportion of the chondritic portion of a body that remains unmelted in our partially differentiated models depends primarily on  $r_2 - r_1$  and  $t_2$ . Bodies with earlier  $t_2$  values produce more radiogenic heat in their chondritic portions, so this material melts more readily when heat from the center of the body passes into this material. It is likely that  $>10\%$  of the radius of the added chondritic material survives metamorphism without melting for  $r_2 - r_1 \gtrsim 10$  km and  $t_2 > 2.5$  Myr after CAI formation. This proportion increases as the thickness of the chondritic layer increases (Figure 5b).

The relatively low internal pressures within asteroid-sized bodies have been proposed to have caused either outward or inward core solidification depending on the core's light element concentration (Williams, 2009). Outward core solidification creates a gravitationally unstable density stratification in the core liquid that has been proposed to have been an efficient mechanism of dynamo generation within cores of asteroid-sized bodies (Bryson et al., 2019; Nimmo, 2009). Inward core solidification has been proposed to have generated dynamo activity through exotic, nonconcentric solidification (Bryson et al., 2017; Neufeld et al., 2019; Ruckriemen et al., 2015). Although many of the details and timings of these processes are uncertain, it is clear that a core cannot generate a magnetic field once it had solidified completely. The timing of the end of core solidification in our model depends primarily on the final radius of the body. Bryson et al. (2019) suggest that bodies with  $r_2 > 170$  km and  $2.0 < t_2 < 2.5$  Myr after CAI formation (period during which radiogenic abundances were high enough that the peak metamorphic temperatures of the H chondrites could be achieved through radiogenic heating) had at least partially molten cores at 100 Myr after CAI formation, so could feasibly have generated magnetic fields when the CZ in Portales Valley recorded its remanence. Our models of partially differentiated bodies with  $r_2$  in this range are capable of producing thermal evolutions with acceptable fits to the measured H chondrite ages (Figure 8). It is therefore possible that partially differentiated bodies with a wide range of radii can explain the measured thermal evolution and remanent magnetization of the H chondrites.

## 4. Discussion

### 4.1. Uncertainties in Field Properties Recovered From the Cloudy Zone

Maurel et al. (2019) outline three sources of uncertainty in paleointensity and paleodirection estimates recovered from XPEEM measurements of the CZ: (1) statistical uncertainty due to analyzing a limited number of islands; (2) measurement uncertainty due to scatter in  $I_A$ ,  $I'_A$ , and  $I''_A$  from location to location (see Supporting Information S1); (3) uncertainties in the bulk Ni concentration of the CZ that impacts the statistical uncertainty by effecting the size of islands when the meteorite cooled through  $320^\circ\text{C}$ . Regarding the statis-

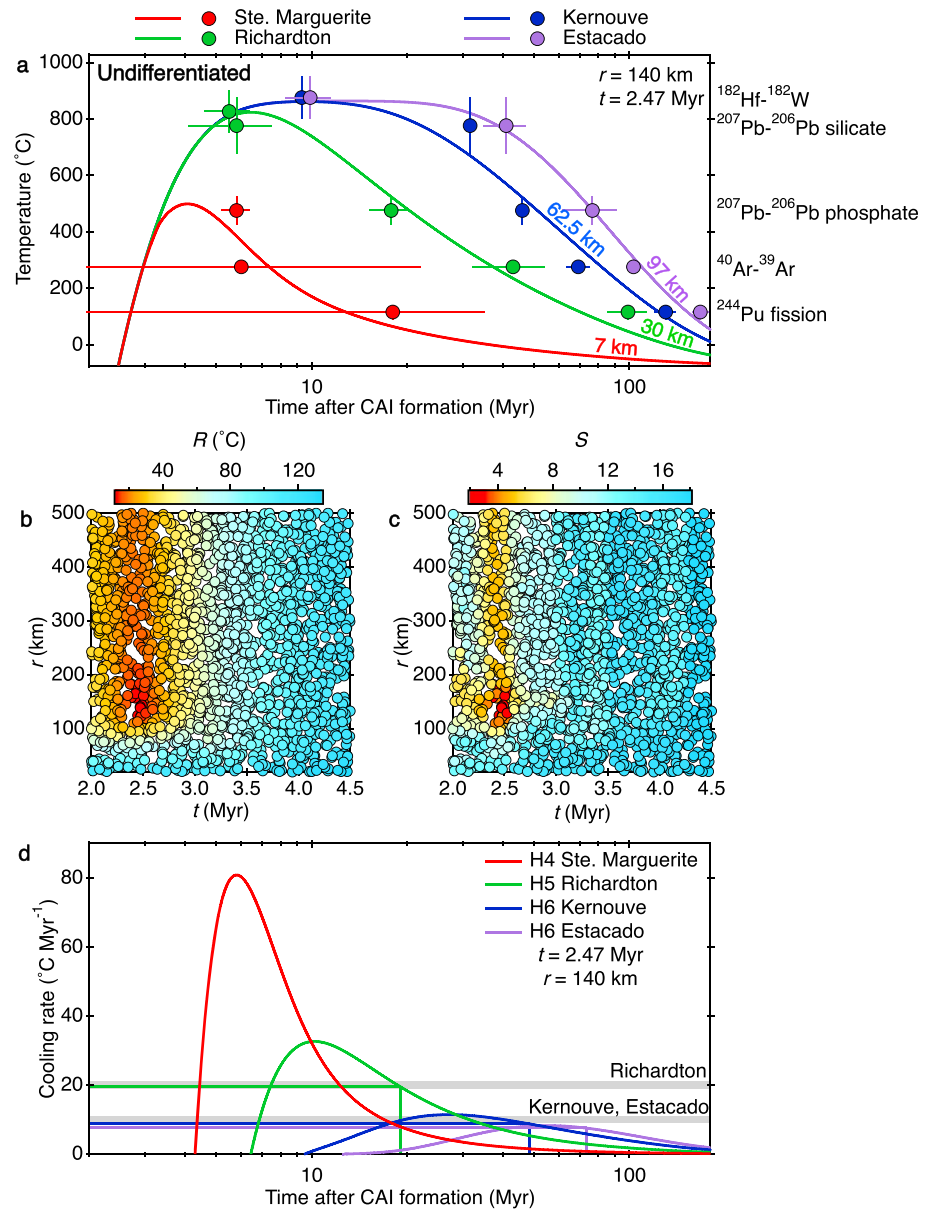


**Figure 7.** Thermal modeling of an undifferentiated H chondrite planetesimal. (a) Measured ages for four well-dated H chondrites (points) and modeled thermal evolutions (solid lines) for a body with parameters that produced the lowest  $R$  value in this model ( $r = 140$  km and  $t = 2.47$  Myr after CAI formation). The depth of each of the modeled thermal evolutions is included next to each curve. The parameters in this model produce an average total residual value of  $R = 12.7$   $^{\circ}\text{C}$  and  $S = 2$ . The geochronological systems are listed on the right of the figure. (b) All combinations of  $r$  and  $t$  color coded by the  $R$  value of the simulation. (c) All combinations of  $r$  and  $t$  color coded by the  $S$  value of the simulation. (d) Calculated cooling rate evolution from the curves in (a). Measured metallographic cooling rates correspond to the cooling rate of a meteorite as it cooled through  $\sim 500$   $^{\circ}\text{C}$  and are depicted by horizontal gray bars (Scott et al., 2014). The time that each meteorite reached this temperature is depicted by the colored vertical lines. The corresponding cooling rate at this time is depicted by the colored horizontal lines. The recovered depth of Ste. Marguerite in this model did not reach 500  $^{\circ}\text{C}$ . CAI = calcium-aluminum-rich inclusion.

tical uncertainty, we analyzed between 47,000 and 190,000 islands along each interface depending on rate of decrease of island size across the CZ in our sample (see section 2.3). According to the analysis of Maurel et al. (2019) and Berndt et al. (2016), and adopting an island radius of 78% of the islands at the present day at the time of tetraenite ordering (Maurel et al., 2019) and a 14- $\mu\text{T}$  field (the average lower limit recovered from the two interfaces we studied), these island numbers produce statistical uncertainties between 2% and 6%. The measurement uncertainty in our recovered paleointensities is 63% (12  $\mu\text{T}$ ) and 78% (7  $\mu\text{T}$ ) for

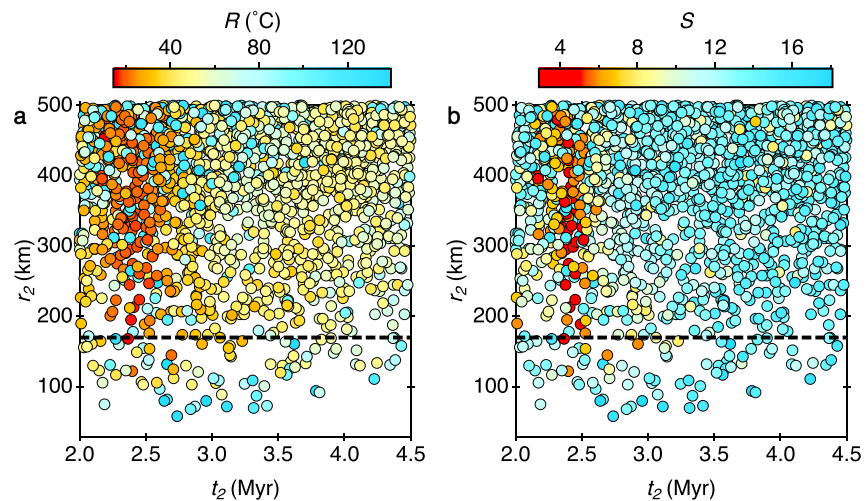


**Figure 8.** All combinations of  $r_2$  and  $t_2$  from our partially differentiated model color coded by (a)  $R$  and (b)  $S$  values of the simulation. The dashed black line depicts  $r_2 = 170$  km, which represents the critical radius above which bodies can have at least partially liquid cores at 100 Myr after CAI formation, so could feasibly have been generating a magnetic field at the time that Portales Valley recorded its remanence (Bryson et al., 2019). A wide range of  $r_2$  values  $>170$  km produce acceptable fits. CAI = calcium-aluminum-rich inclusion.

interfaces A and B, respectively. These values were calculated from the standard deviations in the paleointensities recovered from each location along each interface (Figure S2 in the Supporting Information) and likely reflect variations in the properties of the X-ray beam and the direction and intensity of magnetostatic interaction fields from location to location. The Ni concentration is typically uncertain to  $\pm 1\%$ , which corresponds to a 15% uncertainty in paleointensity (Maurel et al., 2019). Together, these three uncertainties yield total maximum uncertainties of 65% (12  $\mu\text{T}$ ) and 80% (7  $\mu\text{T}$ ) for interface A and B, respectively. These values are dominated by the measurement uncertainty. These total errors are inconsistent with a recovered paleointensity of 0  $\mu\text{T}$ , so our data indicate that the CZ in Portales Valley experienced a field when its islands ordered to form tetrataenite. This conclusion is supported by the range of possible field intensities we calculate from simulated island magnetization configurations expected in the absence of a field (Figure 4).

Another potentially significant source of uncertainty not included in the approach outlined by Maurel et al. (2019) or section 2.3 is island-island magnetostatic interactions. The proximity of the islands in the CZ means that fields emanating from one island could influence the magnetization of neighboring islands. This is almost certainly the case among the coarsest islands, which are separated by distances less than their size. If the underlying CZ island magnetization is random (expected configuration in the absence of an external field), this interaction field is also expected to be randomly oriented across the CZ. This field is therefore not expected to impart a uniform remanence across the CZ from location to location and certainly not from interface to interface. This prediction is verified by the results of Nichols et al. (2016, 2018), who recovered random island magnetization directions and very weak paleointensities (probably  $<1$   $\mu\text{T}$  and certainly within error of zero; Maurel et al., 2019) from younger pallasites and IAB iron meteorites. This observation demonstrates that interactions between islands do not introduce uniform remanences across the CZ. In the presence of an external field, the field experienced by each island across a meteorite is likely a combination of this uniform external field and the local interaction field experienced by each island. In this scenario, it is possible that the remanence carried by the CZ contains a uniform component imparted by the external field. Importantly, the extent of the uniformity introduced by the external field could be influenced and possibly reduced by the local interaction fields. A detailed micromagnetic study of the role of interaction fields on CZ island magnetization has yet to be conducted, so their effect is not included in the paleointensity recovery approach detailed in section 2.3. Importantly, interactions could potentially represent a significant source of uncertainty in our recovered paleointensities. If a future study quantifies the effect of these interactions on the magnetization of the CZ, we could use this result to recover more reliable paleointensities from the data presented in the current study. Regardless of the uncertainties associated with magnetostatic interactions, our observation of relatively uniform paleodirections from location to location and interface to interface as well as our recovered nonzero paleointensities are not expected in the absence of a field, indicating that



the CZ in Portales Valley experienced a field when it chemically ordered. Crucially, the key conclusions we draw regarding the partially differentiated state of the H chondrite parent body rely only on Portales Valley having experienced an ancient field, rather than the paleointensity of this field. Hence, the reliability of this conclusion is not affected by uncertainties introduced by island-island magnetostatic interactions.

#### 4.2. Nature of the Field That Magnetized Portales Valley

The unidirectional remanence we measured in Portales Valley indicates that this meteorite recorded a relatively long-lived field (tens to hundreds of years) compared to the lifetime of impact-generated fields and the timescale of variations in the solar wind field at  $\sim 100$  Myr after CAI formation over a long period.

The small values of the average XMCD intensities extracted from the CZ along both interfaces imply that the NRM is a small percentage of the saturation magnetization, indicating that the magnetization of the CZ in our sample of Portales Valley has not been overprinted by a hand magnet (see results of Gattacceca & Rochette, 2004, for examples of strong remanences in overprinted meteorites). Furthermore, the coercivity of tetrataenite in the CZ ranges from 0.2 to  $>2.0$  T (Bryson, Church, et al., 2014; Néel et al., 1964; Uehara et al., 2011), requiring direct exposure to a very strong rare Earth magnet to alter its remanence. If our sample had been remagnetized by such a hand magnet, we would expect to recover paleointensities in this range. These values are orders of magnitude more intense than the values we recover, further supporting the pristine nature of the NRM carried by our sample of Portales Valley.

It has been suggested previously that the remanence carried by other chondrites could have been imparted by fields generated by the nebula (Cisowski, 1987), the solar wind (Tarduno et al., 2017) or impacts (Muxworthy et al., 2017). The young age of NRM acquisition in Portales Valley ( $\sim 100$  Myr after CAI formation; Bogard & Garrison, 2009) rules out direct magnetization by the nebular field, which had dissipated by  $<3.8$ – $4.8$  Myr after CAI formation (Gattacceca et al., 2016; Wang et al., 2017). The longevity of the recording period in Portales Valley (likely tens to hundreds of years) excludes direct magnetization by the solar wind field, which varies in orientation over a period of just a few days, resulting in a time-averaged intensity during the early solar system  $>3$  orders of magnitude weaker than our recovered paleointensities (Oran et al., 2018). Additionally, Nichols et al. (2016, 2018) recovered random magnetization directions and very weak paleointensities from XPEEM measurements of young pallasites and the IAB iron meteorites. These meteorites experienced the solar wind field at a broadly similar time to Portales Valley, so this weak remanence demonstrates that the solar wind does not impart a recoverable remanence to the CZ. Prolonged remanence acquisition by the CZ also rules out transient fields generated by impacts, which are expected to last  $\lesssim 10$  s on asteroid-sized bodies (e.g., Crawford & Schultz, 2000). Furthermore, Portales Valley contains annealed microstructural evidence that it last experienced a significant impact ( $>5$  GPa) when it was  $>800$ – $1000$  °C (Ruzicka et al., 2015), above the Curie temperature of any of the magnetic phases found in this meteorite (Rochette et al., 2003, 2008). Therefore, Portales Valley was incapable of recording a remanence of any magnetic fields it may have experienced immediately following this impact. Finally, the CZ islands recorded a new remanence as they ordered to form tetrataenite (Einsle et al., 2018), meaning that, even in the extremely unlikely and unexpected scenario that the parent taenite phase had somehow acquired a remanence, this remanence is not reflected in the magnetization of the tetrataenite islands.

It is conceivable that a remanence imparted by an external field source to the early (first 5–10 Myr of the solar system) H chondrite crust could have generated a static remanent field that subsequently imparted a remanence to the CZ in Portales Valley (see Fu et al., 2012, for an example of a meteorite that has been proposed to have been magnetized by such a field). To assess this possibility, we characterized the magnetization of the H4 chondrite Forest Vale (summarized in Table S2 in the supporting information), which cooled sufficiently quickly ( $10,000$  °C/Myr through  $\sim 500$  °C) that it preserved the magnetic properties of the H chondrite crust from this early period (Gattacceca et al., 2014; Scott et al., 2014). Our alternating field (AF) demagnetization measurements (Kirschvink, 1980, 2008; Stephenson, 1993; Tauxe & Staudigel, 2004, 1993; Weiss & Tikoo, 2014), viscous relaxation measurements, and stray field calculations demonstrate that this meteorite can only acquire a low-coercivity anhysteretic remanent magnetization (an analog for thermoremanent magnetization) that is weak, unstable, and easily susceptible to pressure demagnetization (Tikoo et al., 2015; see Supporting Information S1). These observations indicate that it is extremely unlikely that the ancient H chondrite crust was capable of acquiring and preserving a crustal remanence and generating a strong and stable remanent field when Portales Valley recorded its remanence, indicating that this phenomenon is not the source of the remanence in Portales Valley.

The longevity and age of the field we recover from Portales Valley are consistent with the expected properties of fields generated by dynamo activity (Bryson et al., 2019; Weiss & Elkins-Tanton, 2013; Weiss et al., 2010). Coupled with the inconsistent properties of this field with potential external sources, this observation indicates that Portales Valley experienced a dynamo field. These fields are generated by the organized advection of molten metal in a planetary core, implying that the H chondrite parent body contained a metallic core. Combined with the unmelted nature of the H chondrites, this observation indicates that the H chondrite parent body contained both unmelted material and material that partially melted and differentiated. This conclusion suggests that the H chondrite parent body was partially differentiated and consisted of an unmelted exterior atop a differentiated interior. Our asteroid thermal modeling demonstrates that such bodies could have formed through incremental accretion and that the thermal evolution of these bodies can be consistent with the measured ages (Figures 5a, 5d, and 5e) and cooling rates (Figure 6) of multiple H chondrites. Additionally, these models demonstrate that the cores of these bodies could have been partially molten (i.e., feasibly capable of generating compositionally driven dynamo fields) at the time Portales Valley recorded a remanence for final radii  $\gtrsim 170$  km (Figure 8). Together, the measured remanent magnetization and thermal evolution of the H chondrite parent body are consistent with a partially differentiated parent asteroid, suggesting that such bodies formed during the early solar system.

Two other pieces of evidence exist that potentially support a partially differentiated H chondrite parent body. First, the IIE iron meteorites contain silicate inclusions with geochemical and isotopic affinities to the H chondrites, indicating that these meteorites originate from metal pools embedded in the mantle of an H chondrite-like body. The lithology of these inclusions range from unmelted and chondrule-bearing to completely molten, providing independent evidence that H chondrite-like parent bodies could possibly be partially differentiated (Weiss & Elkins-Tanton, 2013). Second, the partially melted nature of Portales Valley supports the partial differentiation of its parent body if this meteorite was heated solely by the decay of  $^{26}\text{Al}$  (Ruzicka et al., 2005).

#### 4.3. Implications of Partially Differentiated Asteroids

Our thermal and magnetic observations are consistent with episodic accretion of chondrules and other chondrite components to form the H chondrite parent body. Johansen et al. (2015) predict that asteroids with radii  $>100$  km likely gained a significant portion of their final mass through the late-stage addition of chondrules atop an initial planetesimal seed. This predicted accretion scenario is extremely similar to asteroid growth mechanism adopted in this study. This predicted size range also agrees with the range we recover for the H chondrite parent body based on both the thermal evolution and the timing of the end of core solidification (Figures 5 and 8), supporting the hypothesis that some asteroids underwent episodic accretion of chondrules.

We assume in our model that both accretion events are instantaneous. Although this accretion timescale is impossible and we adopted it for simplicity, the similarity in chondrule size and chemistry across different members of the same chondrite group and the estimated turbulent diffusion timescales during nebula accretion indicate that chondritic material accreted over short periods ( $<0.2$  Myr; Alexander, 2005). Indeed, previous modeling studies suggest the thermal evolution of bodies that formed by gradual accretion over short time periods can agree with that measured from the H chondrites (Monnereau et al., 2013). Given our results suggest that instantaneous chondrule accretion at times between 2.3 and 2.5 Myr after CAI formation produces acceptable fits to the measured H chondrite ages, we expect that a gradual second accretion event spanning  $\sim 2.3$ – $2.5$  Myr after CAI formation will introduce a similar amount of heat to the chondritic portion of the final body, so likely also produce acceptable fits to the measured H chondrite thermal evolutions. As our recovered range of  $t_2$  values that produce acceptable fits is close to the end of our range of possible  $t_1$  times (0.0–2.0 Myr after CAI formation), it may be possible that one prolonged accretion event lasting from sometime  $<2.0$  to  $\sim 2.5$  Myr after CAI formation could also produce partially differentiated bodies (Lichtenberg et al., 2018) that could be consistent with the measured magnetization and thermal evolution of the H chondrites.

If the accretion events in the incremental scenario supported by this study differed in time by  $10^5$ – $10^6$  years, it is possible that the material added to the body during each event could originate from separate chemical and isotopic reservoirs present at different times and locations in the early solar system. This accretion history challenges a central common assumption of modern meteorite classification schemes that meteorite groups are samples of distinct parent planetesimals that form from material originating from individual

reservoirs (Weiss & Elkins-Tanton, 2013; Wiesberg et al., 2006). Instead, it is possible that incremental accretion could produce chondrites and achondrites that originate from the same, radially layered, partially differentiated body that need not share the same genetic chemical and isotopic origin. As such, it is possible that the great diversity of meteorite groups reflected in these classification schemes may belie underlying simpler genetic relationships between these groups.

Finally, our observations suggest that the surface of an asteroid may not be representative of its internal structure and composition. Specifically, our modeling suggests that asteroids with chondritic surfaces could have varying extents of internal melting and differentiation. The different internal structures in partially differentiated and undifferentiated bodies would produce different density profiles with depth throughout these bodies, so it may be possible to use this property to distinguish between these types of asteroid and assess the extent of internal melting and differentiation within bodies with primitive surfaces (Weiss et al., 2012).

## 5. Conclusions

- The parent asteroids of chondrites are thought not to have partially melted through endogenic heating and hence are not believed to have undergone igneous differentiation and core formation.
- We measured the magnetic remanence carried in metal veins in the H6 ordinary chondrite Portales Valley using synchrotron X-ray microscopy. We found that nanostructures in these veins recorded a spatially-uniform magnetic remanence as they formed during low-temperature recrystallization over a relatively long period (tens to hundreds of years) at  $\sim 100$  Myr after CAI formation. This observation indicates this meteorite experienced a late-stage and relatively long-lived magnetic field.
- The longevity and age of this field are inconsistent with external sources of magnetic field such as the nebula, solar wind, or impacts. Instead, these properties are consistent with those expected for fields generated by internal core dynamo activity, indicating that the H chondrite parent body contained an advancing metallic core and was, therefore, partially differentiated.
- Thermal evolution models demonstrate that incremental accretion over  $10^5$ – $10^6$  years can result in partially differentiated bodies with thermal histories that agree with the measured ages and cooling rates of multiple H chondrites. These models also demonstrate that such bodies can have partially molten cores at  $\sim 100$  Myr after CAI formation, so could have feasibly generated a dynamo field at the time that Portales Valley recorded its remanence.
- These observations support a spectrum of internal differentiation within some asteroids with chondritic surfaces, suggest that accretion could have been a prolonged process and hint that a single body could be composed of material from multiple chemical and isotopic reservoirs present in the early solar system, permitting diverse meteorite groups to possibly originate from a common, radially-heterogeneous parent asteroid.

## Acknowledgments

We thank C. Nichols, R. Harrison, and E. Lima for assistance and helpful discussions. J. A. thanks the Caltech Summer Undergraduate Research Fellowship program. J. F. J. B. and B. P. W. thank the NASA Solar System Exploration Research Virtual Institute grant NNA14AB01A, the NASA Solar System Workings Program (grant NNX15AL62G), and Thomas F. Peterson, Jr. for support. J. F. J. B. would also like to thank St. John's College, University of Cambridge for funding. The Advanced Light Source is supported by the Director, Office of Science, Office of Basic Energy Sciences of the U.S. D.O.E. under contract DE-AC02-05CH11231. We would like to thank the Natural History Museum, London, and the U.S. National Museum for loaning us meteorites. The data in this paper can be found on the MagIC database (<https://www2.earthref.org/MagIC>).

## References

- Alexander, C. M. O. (2005). From supernovae to planets: The view from meteorites and interplanetary dust particles, *Chondrites and the protoplanetary disk* (pp. 972–1002). Hawai'i: Astronomical Society of the Pacific.
- Amelin, Y., Ghosh, A., & Rotenberg, E. (2005). Unraveling the evolution of chondrite parent asteroids by precise U-Pb dating and thermal modeling. *Geochimica et Cosmochimica Acta*, 69, 505–518.
- Berndt, T., Muxworthy, A. R., & Fabian, K. (2016). Does size matter? Statistical limits of paleomagnetic field reconstruction from small rock specimens. *Journal of Geophysical Research: Solid Earth*, 121, 15–26. <https://doi.org/10.1002/2015JB012441>
- Blackburn, T., Alexander, C. M. O., Carlson, R., & Elkins-Tanton, L. T. (2017). The accretion and impact history of the ordinary chondrite parent bodies. *Geochimica et Cosmochimica Acta*, 200, 201–217.
- Blinova, A., Amelin, Y., & Samson, C. (2007). Constraints on the cooling history of the H-chondrite parent body from phosphate and chondrule Pb-isotopic dates from Estacado. *Meteoritics and Planetary Science*, 42, 1337–1350.
- Bogard, D. D., & Garrison, D. H. (2009). Ar–Ar and I–Xe ages and thermal histories of three unusual metal-rich meteorites. *Geochimica et Cosmochimica Acta*, 73, 6965–6983.
- Bouvier, A., Blichert-Toft, J., Moynier, F., Vervoort, J. D., & Albarede, F. (2007). Pb–Pb dating constraints on the accretion and cooling history of chondrites. *Geochimica et Cosmochimica Acta*, 71, 1583–1604.
- Bryson, J. F. J., Church, N. S., Kasama, T., & Harrison, R. J. (2014). Nanomagnetic intergrowths in Fe–Ni meteoritic metal: The potential for time-resolved records of planetesimal dynamo fields. *Earth and Planetary Science Letters*, 388, 237–248.
- Bryson, J. F. J., Herrero-Albillos, J., Kronast, F., Ghidini, M., Redfern, S. A. T., van der Laan, G., & Harrison, R. J. (2014). Nanopaleomagnetism of meteoritic Fe–Ni studied using X-ray photoemission electron microscopy. *Earth and Planetary Science Letters*, 396, 125–133.
- Bryson, J. F. J., Neufeld, J. A., & Nimmo, F. (2019). Constraints on asteroid magnetic field evolution and the radii of meteorite parent bodies from thermal modelling. *Earth and Planetary Science Letters*, 521, 68–78. <https://doi.org/10.1016/j.epsl.2019.05.046>



- Bryson, J. F. J., Nichols, C. I. O., Herrero-Albillos, J., Kronast, F., Kasama, T., Alimadadi, H., & Harrison, R. J. (2015). Long-lived magnetism from solidification-driven convection on the pallasite parent body. *Nature*, 517, 472–475.
- Bryson, J. F. J., Weiss, B. P., Harrison, R. J., Herrero-Albillos, J., & Kronast, F. (2017). Paleomagnetic evidence for dynamo activity driven by inward crystallisation of a metallic asteroid. *Earth and Planetary Science Letters*, 472, 152–163.
- Carpözen, L., Weiss, B. P., Elkins-Tanton, L. T., Shuster, D. L., Ebel, D. S., & Gattacceca, J. (2011). Magnetic evidence for a partially differentiated carbonaceous chondrite parent body. *Proceedings of the National Academy of Sciences*, 108, 6386–6389.
- Cisowski, S. M. (1987). Magnetism of meteorites. In *Geomagnetism*, J. A. Jacobs (Ed.) (Vol. 2, 525–560). London: Academic Press.
- Crawford, D., & Schultz, P. (2000). Electrostatically charged impact ejecta and implications for lunar paleomagnetism, Houston, Texas. Abstract 1849.
- Dos Santos, E., Gattacceca, J., Rochette, P., Fillion, G., & Scorzelli, R. B. (2015). Kinetics of tetraenaite disordering. *Journal of Magnetism and Magnetic Materials*, 375, 234–241.
- Doyle, P. M., Jogo, K., Nagashima, K., Krot, A. N., Wakita, S., Ciesla, F. J., & Hutcheon, I. D. (2015). Early aqueous activity on the ordinary and carbonaceous chondrite parent bodies recorded by fayalite. *Nature Communications*, 6, 7444.
- Einsle, J. F., Eggeman, A. S., Martineau, B. H., Saghi, Z., Collins, S. M., Blukis, R., & Harrison, R. J. (2018). Nanomagnetic properties of the meteorite cloudy zone. *Proceedings of the National Academy of Sciences*, 115, E11436–E11445.
- Elkins-Tanton, L. T., Weiss, B. P., & Zuber, M. T. (2011). Chondrites as samples of differentiated planetesimals. *Earth and Planetary Science Letters*, 305, 1–10.
- Fu, R. R., Lima, E. A., Weiss, B. P., & 54–66 (2014). No nebular magnetization in the Allende CV carbonaceous chondrite. *Earth and Planetary Science Letters*, 404.
- Fu, R. R., Weiss, B. P., Shuster, D. L., Gattacceca, J., Grove, T. L., Suavet, C., & Kuan, A. T. (2012). An ancient core dynamo in asteroid vesta. *Science*, 338, 238–241.
- Gattacceca, J., & Rochette, P. (2004). Toward a robust normalized magnetic paleointensity method applied to meteorites. *Earth and Planetary Science Letters*, 227, 377–393.
- Gattacceca, J., Suavet, C., Rochette, P., Weiss, B. P., Winklhofer, M., Uehara, M., & Friedrich, J. M. (2014). Metal phases in ordinary chondrites: Magnetic hysteresis properties and implications for thermal history. *Meteoritics and Planetary Science*, 49, 652–676.
- Gattacceca, J., Weiss, B. P., & Gounelle, M. (2016). New constraints on the magnetic history of the CV parent body and the solar nebula from the Kaba meteorite. *Earth and Planetary Science Letters*, 455, 166–175.
- Goldstein, J. I., Scott, E. R. D., & Chabot, N. L. (2009). Iron meteorites: Crystallization, thermal history, parent bodies, and origin. *Chemie der Erde - Geochemistry*, 69, 293–325.
- Henke, S., Gail, H. P., Trieloff, M., & Schwartz, W. H. (2013). Thermal evolution model for the H chondrite asteroid—Instantaneous formation versus protracted accretion. *Icarus*, 226, 212–228.
- Hevey, P. J., & Sanders, I. S. (2006). A model for planetesimal meltdown by  $^{26}\text{Al}$  and its implications for meteorite parent bodies. *Meteoritics and Planetary Science*, 41, 95–106.
- Johansen, A., Low, M. M., Lacerda, P., & Bizzarro, M. (2015). Growth of asteroids, planetary embryos, and Kuiper belt objects by chondrule accretion. *Science Advances*, 17, e1500109.
- Kirschvink, J. L. (1980). The least-squares line and plane and the analysis of paleomagnetic data. *Geophysical Journal International*, 62, 699–718.
- Kirschvink, J. L., Kopp, R. E., Raub, T. D., Baumgartner, C. T., & Holt, J. W. (2008). Rapid, precise, and high-sensitivity acquisition of paleomagnetic and rock-magnetic data: Development of a low-noise automatic sample changing system for superconducting rock magnetometers. *Geochemistry, Geophysics, Geosystems*, 9, Q05Y01. <https://doi.org/10.1029/2007GC001856>
- Kleine, T., Touboul, M., van Orman, J. A., Bourdon, B., Maden, C., Mezger, K., & Halliday, A. N. (2008). Hf-W thermochronometry: Closure temperature and constraints on the accretion and cooling history of the H chondrite parent body. *Earth and Planetary Science Letters*, 270, 106–118.
- Lichtenberg, T., Golabek, G. J., Dullemond, C. P., Schönbächler, M., Gerya, T. V., & Meyer, M. R. (2018). Impact splash chondrule formation during planetesimal recycling. *Icarus*, 302, 27–43.
- Maurel, C., Bryson, J. F. J., Weiss, B. P., & Scholl, A. (2018). Paleomagnetic evidence for a layered partially differentiated iron-meteorite parent body. In *Lunar and Planetary Science Conference XLIX*. Abstract 1171, Houston, Texas.
- Maurel, C., Weiss, B. P., & Bryson, J. F. J. (2019). Meteorite cloudy zone formation as a quantitative indicator of paleomagnetic field intensities and cooling rates on planetesimals. *Earth and Planetary Science Letters*, 513, 166–175.
- Monnereau, M., Toplis, M. J., Baratoux, C., & Guignard, J. (2013). Thermal history of the H-chondrite parent body: Implications for the metamorphic grade and accretionary time-scales. *Geochimica et Cosmochimica Acta*, 119, 302–321.
- Morris, D. G., Besag, F. M. C., & Smallman, R. E. (1974). Ordering and disordering in  $\text{Cu}_3\text{Au}$ . *The Philosophical Magazine: A Journal of Theoretical Experimental and Applied Physics*, 29, 43–57.
- Muxworthy, A. R., Bland, P. A., Davison, T. M., Moore, J., Collins, G. S., & Ciesla, F. J. (2017). Evidence for an impact-induced magnetic fabric in Allende, and exogenous alternatives to the core dynamo theory for Allende magnetization. *Meteoritics and Planetary Science*, 52, 2132–2146. <https://doi.org/10.1111/maps.12918>
- Néel, L., Pauleve, J., Pauthenet, R., Laugier, J., & Dautreppe, D. (1964). Magnetic properties of an iron-nickel single crystal ordered by neutron bombardment. *Journal of Applied Physics*, 35, 873–876.
- Neufeld, J. A., Bryson, J. F. J., & Nimmo, F. (2019). The top-down solidification of iron asteroids driving dynamo evolution. *Journal of Geophysical Research: Planets*, 124, 1331–1356.
- Nichols, C. I. O., Bryson, J. F. J., Herrero-Albillos, J., Kronast, F., Nimmo, F., & Harrison, R. J. (2016). Pallasite paleomagnetism: Quiescence of a core dynamo. *Earth and Planetary Science Letters*, 441, 103–112.
- Nichols, C. I. O., Krakow, R., Herrero-Albillos, J., Kronast, F., Northwood-Smith, G., & Harrison, R. J. (2018). Microstructural and paleomagnetic insight into the cooling history of the IAB parent body. *Geochimica et Cosmochimica Acta*, 229, 1–19.
- Nimmo, F. (2009). Energetics of asteroid dynamos and the role of compositional convection. *Geophysical Research Letters*, 36, L10210. <https://doi.org/10.1029/2009GL037997>
- Opeil, C. P., Consolmagno, G. J., Safarik, D. J., & Britt, D. T. (2012). Stony meteorite thermal properties and their relationship with meteorite chemical and physical states. *Meteoritics and Planetary Science*, 47, 319–329.
- Oran, R., Weiss, B. P., & Cohen, O. (2018). Were chondrites magnetized by the early solar wind? *Earth and Planetary Science Letters*, 492, 222–231.
- Rochette, P., Gattacceca, J., Bonal, L., Bourrot-Denise, M., Chevier, V., Clerc, J. P., & Skripnik, A. (2008). Magnetic classification of stony meteorites: 2. Non-ordinary chondrites. *Meteoritics and Planetary Science*, 43, 959–980.

- Rochette, P., Sagnotti, L., Bourot-Denise, M., Consolmagno, G., Folco, L., Gattacceca, J., & Pesonen, L. (2003). Magnetic classification of stony meteorites: 1. Ordinary chondrites. *Meteoritics and Planetary Science*, 38(2), 251–268.
- Rubin, A. E. (2004). Postshock annealing and postannealing shock in equilibrated ordinary chondrites: implications for the thermal and shock histories of chondritic asteroids. *Geochimica et Cosmochimica Acta*, 68, 673–689.
- Ruckriemen, T., Breuer, D., & Spohn, T. (2015). The Fe snow regime in Ganymede's core: A deep-seated dynamo below a stable snow zone. *Journal of Geophysical Research: Planets*, 120, 1095–1118. <https://doi.org/10.1002/2014JE004781>
- Ruzicka, A., Hugo, R., & Hutson, M. (2015). Deformation and thermal histories of ordinary chondrites: Evidence for post-deformation annealing and syn-metamorphic shock. *Geochimica et Cosmochimica Acta*, 163, 219–233.
- Ruzicka, A., Killgore, M., Mittlefehldt, D. W., & Fries, M. D. (2005). Portales Valley: Petrology of a metallic-melt meteorite breccia. *Meteoritics and Planetary Science*, 40, 261–295.
- Scott, E. R. D., Krot, T. V., Goldstein, J. I., & Wakita, S. (2014). Thermal and impact history of the H chondrite parent asteroid during metamorphism: Constraints from metallic Fe-Ni. *Geochimica et Cosmochimica Acta*, 136, 13–37.
- Shah, J., Bates, H. C., Muxworthy, A. R., Hezel, D. C., Russell, S. S., & Genge, M. J. (2017). Long-lived magnetism on chondrite parent bodies. *Earth and Planetary Science Letters*, 475, 106–118.
- Stephenson, A. (1993). Three-axis static alternating field demagnetization of rocks and the identification of natural remanent magnetization, gyroremanent magnetization, and anisotropy. *Journal of Geophysical Research*, 98, 373–381.
- Stöffler, D., Keil, K., & Scott, E. R. D. (1991). Shock metamorphism of ordinary chondrites. *Geochimica et Cosmochimica Acta*, 55, 3845–3867.
- Tarduno, J. A., O'Brien, T. M., Blackman, E. G., & Smirnov, A. V. (2017). Magnetization of CV meteorites in the absence of a parent body core dynamo. In *Lunar and Planetary Science Conference XLVIII*. Abstract 2850.
- Tauxe, L., & Staudigel, H. (2004). Strength of the geomagnetic field in the Cretaceous Normal Superchron: New data from submarine basaltic glass of the Troodos Ophiolite. *Geochemistry, Geophysics, Geosystems*, 5, Q02H06. <https://doi.org/10.1029/2003GC000635>
- Tikoo, S. M., Gattacceca, J., Swanson-Hysell, N. L., & Weiss, B. P. (2015). Preservation and detectability of shock-induced magnetization. *Journal of Geophysical Research: Planets*, 120, 1461–1475. <https://doi.org/10.1002/2015JE004840>
- Trieloff, M., Jessberger, E. K., Herrwerth, I., Hopp, J., Fieni, C., Ghelis, M., & Pellas, P. (2003). Structure and thermal history of the H-chondrite parent asteroid revealed by thermochronometry. *Nature*, 422, 502–506.
- Uehara, M., Gattacceca, J., Leroux, H., Jacob, D., & van der Beek, C. J. (2011). Magnetic microstructures of metal grains in equilibrated ordinary chondrites and implications for paleomagnetism of meteorites. *Earth and Planetary Science Letters*, 306, 241–252.
- Wang, H., Weiss, B. P., Bai, X. N., Downey, B. G., Wang, J., Wang, J., & Zucolotto, M. E. (2017). Lifetime of the solar nebula constrained by meteorite paleomagnetism. *Science*, 355, 623–627.
- Warren, P. H. (2011). Ejecta-megaregolith accumulation on planetesimals and large asteroids. *Meteoritics and Planetary Science*, 46, 53–78.
- Weiss, B. P., & Elkins-Tanton, L. T. (2013). Differentiated planetesimals and the parent bodies of chondrites. *Annual Review of Earth and Planetary Sciences*, 41, 529–560.
- Weiss, B. P., Elkins-Tanton, L. T., Barucci, M. A., Sierks, H., Snodgrass, C., Vincent, J. B., & Schulz, R. (2012). Possible evidence for partial differentiation of asteroid Lutetia from Rosetta. *Planetary and Space Science*, 66, 137–146.
- Weiss, B. P., Gattacceca, J., Stanley, S., Rochette, P., & Christensen, U. R. (2010). Paleomagnetic records of meteorites and early planetesimal differentiation. *Space Science Reviews*, 152, 341–390.
- Weiss, B. P., & Tikoo, S. M. (2014). The lunar dynamo. *Science*, 346, 1246753.
- Wiesberg, M. K., McCoy, T. J., & Krot, A. N. (2006). Systematics and evaluation of meteorite classification, *Meteorites and the Early Solar System II*. Tucson: University of Arizona Press, pp. 19–52.
- Williams, Q. (2009). Bottom-up versus top-down solidification of the cores of small solar system bodies: Constraints on paradoxical cores. *Earth and Planetary Science Letters*, 284, 564–569.